Pergamon

Geochimica et Cosmochimica Acta, Vol. 67, No. 15, pp. 2879–2891, 2003

0016-7037/03 $30.00 + .00

doi:10.1016/S0016-7037(03)00080-2

High precision iron isotope measurements of meteoritic material by cold plasma ICP-MS

K. KEHM,* E. H. HAURI, C. M. O'D. ALEXANDER, and R. W. CARLSON

Department of Terrestrial Magnetism, Carnegie Institution of Washington, 5241 Broad Branch Rd., N.W., Washington, D.C. 20015 USA

(*Received February* 20, 2002; *accepted in revised form December* 19, 2002)

Abstract—The first cold plasma ICP-MS (inductively coupled plasma mass spectrometer) Fe isotope study is described. Application of this technique to the analyses of Fe isotopes in a number of meteorites is also reported. The measurement technique relies on reduced temperature operation of the ICP source to eliminate pervasive molecular interferences from Ar complexes associated with conventional ICP-MS. Instrumental mass bias corrections are performed by sample-standard bracketing and using Cu as an external mass bias drift monitor. Repeated measurements of a terrestrial basalt reference sample indicate an external reproducibility of ± 0.06 ‰ for δ^{56}Fe and ± 0.25 ‰ for δ^{58}Fe (1 σ). The measured iron isotopic compositions of various bulk meteorites, including irons, chondrites and pallasites are identical, within error, to the composition of our terrestrial basalt reference sample suggesting that iron mass fractionation during planet formation and differentiation was non-existent. Iron isotope compositions measured for eight chondrules from the unequilibrated ordinary chondrite Tieschitz range from -0.5 ‰ $< \delta^{56}Fe_{chondrules} < 0.0$ ‰ relative to the terrestrial/meteorite average. Mechanisms for fractionating iron in these chondrules are discussed. *Copyright © 2003 Elsevier Science Ltd*

1. INTRODUCTION

Iron is one of the most abundant rock-forming elements in the solar system, occurring in meteorites in metallic form, as well as in lithophile and chalcophile associations. Despite its abundance, the isotopic behavior of iron in meteorites has not been adequately characterized, owing partly to the inherent difficulty in precisely measuring iron isotopes with established mass spectrometry techniques.

Variations in the isotopic composition of iron can plausibly result from the presence of unequilibrated anomalous presolar material, cosmic ray spallation, and mass-dependent fractionation. Though iron is relatively volatile and was probably largely isotopically equilibrated in the nebula, nucleosynthetic enrichments in the neutron-rich isotope ^{58}Fe persist in some refractory inclusions in carbonaceous chondrites (Völkening and Papanastassiou, 1989). Preserved iron isotopic mass fractionation may also occur in meteorites (Kehm et al., 2001a, 2001b, 2001c, Zhu et al., 2001), as appears to be the case for neighboring transition elements Cu and Zn (Luck et al., 2001). In particular, Zhu et al. (2001), who carried out the first detailed high-precision survey of iron isotope compositions in meteorites using conventional ICP-MS, measured a range of mass fractionated iron compositions among bulk meteorites and, in some cases, among chondrules and matrix samples from the same meteorite. Such effects can result from temperature-sensitive isotope exchange reactions and kinetic processes, and therefore may reflect conditions in the solar nebula and on meteorite parent bodies.

Of additional interest is the recent identification of mass-fractionated Fe in low temperature minerals on Earth, which have been tentatively attributed to metabolic processing by microorganisms (Beard et al., 1999). Though the sources of these variations are the subject of continuing debate (Mandernack et al., 1999; Zhu et al., 2000; Anbar et al., 2000; Sharma et al., 2001), this suggestion has generated considerable attention in the geochemical community because of the possibility that Fe mass fractionation may serve as a tracer for microbial activity. In the context of this work, meteorites provide a useful alternative setting in which to study abiological mass fractionation because they are devoid of biologic processing.

For a given element, isotopic mass fractionation generally scales as a function of the relative isotopic mass dispersion ($^{\Delta M}/_{M}$) (e.g., Bigeleisen, 1965). Thus natural mass fractionation becomes increasingly difficult to detect in heavier elements. Analyses of isotopic mass fractionation in natural samples, so called stable isotope studies, have been largely relegated to light elements such as H, C, N, O, and S. Only recently have the transition metals and heavier elements become accessible for stable isotope research, thanks in large part to advancements in instrumentation and techniques.

Crucial for resolving stable isotope effects is the ability to distinguish fractionation induced in the laboratory from that present in the sample. For iron, mass fractionation induced by the mass spectrometer can be orders of magnitude larger than the fractionation signal in the sample. Thermal ionization mass spectrometry (TIMS) has traditionally been used for isotopic analyses of iron and other mineral-forming elements. However, TIMS requires a cumbersome double isotope spiking technique to accurately correct for instrumental mass discrimination and furthermore suffers from poor ionization efficiency for iron (Johnson and Beard, 1999). In contrast, inductively coupled plasma mass spectrometers (ICP-MS) efficiently ionize nearly all elements in the Ar source plasma. Moreover, external instrumental mass bias corrections are possible by sample-standard bracketing and/or simultaneous isotopic analysis of a standard element in solution with the sample (e.g., Walder et al., 1993).

Unfortunately, Ar source plasmas are notorious for the copious production of ArO^+, ArN^+ and $ArOH^+$, which present isobaric interferences at masses 54, 56, 57 and 58 where iron

* Author to whom correspondence should be addressed (kehm@dtm.ciw.edu).

isotopes reside. Several techniques have been employed to overcome this problem. Some degree of argide reduction can be achieved using a sample desolvation nebulizer system. Corrections for residual interferences are then performed by sample/standard normalization (Zhu et al., 2000, Anbar et al., 2000). This requires matching of both the Fe signals and interference levels in samples and standards. Ideally this approach permits precise Fe measurements without extraordinary efforts to eliminate the argides. Recently collision cell technology has been used to crack molecular interferences created in the source plasma before passing the beam through the spectrometer mass analyzer. Application of this technique to iron analysis is currently underway (Johnson et al., 2002). The newest generation of high-mass resolution ICP-MS instruments also shows promise in the ability to perform precise iron isotope measurements while simultaneously resolving argide interferences (e.g., Weyer et al., 2001).

We have developed a technique for high-precision iron isotope analyses using ICP-MS that relies on so-called 'cold plasma' operating conditions to eliminate argide interferences. Cold plasma ICP-MS was first attempted by Jiang et al. (1988) who realized that a reduction in plasma operating temperature greatly reduced the pervasive ^{40}Ar background signal, permitting analysis of ^{40}K. Subsequently several other authors explored cold plasma ICP-MS techniques to improve abundance measurements of the elements normally obstructed by argide interferences, including Fe, Ca and K (see Tanner, 1995, and references therein).

Herein we describe the first efforts to measure iron isotopes in natural samples using cold plasma ICP-MS. This paper represents the culmination of work presented by Kehm et al. (2001a, 2001b, 2001c).

2. EXPERIMENTAL

2.1. Samples

A number of iron meteorites, silicates and iron from two pallasites, several chondrites, and a suite of chondrules from the ordinary chondrite Tieschitz where analyzed in this initial study, along with multiple aliquots of a terrestrial basalt (described below). Slabs of Fe-Ni alloy ($\sim$ 1 g) were cut from larger sawed fragments of each iron meteorite and the pallasite Brenham, washed in 5% nitric acid for 2 min, dried and weighed. Silicate fragments were hand-picked from a crushed sample of the pallasite Admire and similarly washed and weighed. Bulk fragments of Orgueil and Allende were prepared in the same way. The sample of Murchison was available in powdered form (USNM #5467) and thus the washing step was skipped for this meteorite. Chondrules were mechanically separated from the Tieschitz meteorite by freeze/thaw disaggregation in water. Round chondrules were selected, washed in dilute nitric for about two minutes, dried and weighed.

2.2. Chemistry

Chemical purification of iron using anion exchange chromatography has been reported by a number of authors (e.g., Strelow, 1980). Isotopic mass fractionation can be caused by incomplete yields from the anion separation column (Anbar et al., 2000). Also, mass fractionation can be induced during measurement due to the presence of contaminant ('matrix') elements in the analyte solution (see below). High resolution, high-yield chemical separation procedures are thus critical for avoiding these potential problems.

Samples were acid dissolved using distilled, ultra-pure reagents. Iron meteorites were dissolved in *aqua regia*. Silicate samples were first exposed to a concentrated HNO_3/HF mixture. Subsequently they were dried down (at temperatures less than about 50° C) and re-dissolved in 6 N HCl to eliminate insoluble fluorides. This mixture was dried. Samples were then re-dissolved in a solution of 9 N HCl + 0.001% H_2O_2 and extensively centrifuged to separate insoluble particles. Centrifugation was particularly important for the chondrite samples, which contain a significant fraction (on the order of $\sim$1%) of insoluables, including organics, some chromite and refractory carbonaceous phases.

Iron separation and purification was achieved by passing bulk solutions through an anion exchange column (AG1-X4 100–200 mesh). At high HCl molarity, Fe(III) is strongly retained on the anion column while significant matrix elements wash through. A small amount of peroxide, a strong oxidant, was added to the sample solutions to suppress conversion of Fe(III) to Fe(II) during the column procedure (cf. van der Walt et al., 1985; Maréchal et al., 1999). Approximately 3 mL of resin (wet volume) were used for 1 mg of Fe. Matrix elements were washed through the resin with 50 mL of 9 N HCl + 0.001% H_2O_2. Iron was eluted with 15 mL of 0.1 N HCl. Subsequently, the eluted Fe was dried down at $<$50° C and re-dissolved in 8 N HNO_3. These solutions were dried down again and re-dissolved in 1.1 N HNO_3. The latter solutions were analyzed by ICP-MS. Yields were estimated for samples with known Fe content by comparing the Fe signal intensities with those of a standard. Iron yields with this technique are conservatively estimated at better than 95%.

2.3. Mass Spectrometry

Isotopic measurements were performed on the Department of Terrestrial Magnetism's VG Axiom multi-collector ICP-MS. As discussed above, argon plasma sources are normally copious producers of polyatomic argide molecules that can interfere with measurements of iron isotopes as well as a number of other elements. Argide elimination requires (1) reduced power ('cold plasma') operation, and (2) the suppression of so called 'secondary discharge', or arcing between the plasma and the sampling interface. In an Ar ICP source, the reduction in plasma temperature shifts the dominant background ion from $^{40}Ar^+$ to NO^+ (Jiang et al., 1988; Tanner, 1995), greatly reducing or effectively eliminating most of the relevant argide interferences. Secondary discharge can occur as a result of capacitive coupling between the load coil and the plasma (e.g., Douglas and Tanner, 1998). In the VG Axiom, capacitive coupling is suppressed by the presence of a grounded metal shield situated between the load coal and the torch.

During these measurements, the RF generator was operated at 600 W, about half of the normal operating power. A conventional concentric Meinhard-style nebulizer was used for sample injection. The sample introduction system consisted of a water-cooled glass cyclonic and spray chamber. Cold plasma argide reduction could not be achieved with a commercial desolvating sample introduction system. The reasons for this are unknown, but could be related to the relative absence of water vapor in the desolvated aerosol; water may play a key role in keeping the plasma cool enough to suppress argide formation. Eliminating argides in cold plasma mode also required high nebulizer gas flow rates (1.1 L/min) and large sampling depths (distance between the torch and the sampling interface cone). These specialized tuning conditions presumably help to maintain a cooler ambient plasma temperature in the sampling zone of the source plasma (Tanner, 1995). During cold plasma operation, the ArO^+ is much less than a part in 10^4 of the ^{56}Fe signal. The ArN^+ contribution to mass 54 is rendered negligible. In contrast, under conventional conditions, argide interferences at masses 54 and 56 can range up to several tens of percent of the corresponding Fe isotope signals at these masses.

Unfortunately there is little or no attenuation of hydroxides in cold plasma mode. Therefore, manual monitoring of K, Ca and Ar, whose isotopes can, in principle, form hydroxide molecules that interfere with Fe, was required. This practice has revealed some variability in the Ca background among different solutions, which seems to be responsible for an observed lack of accuracy and precision in the measured ^{57}Fe/^{54}Fe ratio. High mass resolution scans in cold plasma mode of the mass 57 region indeed confirm the presence of an unsuppressed hydroxide. To better understand the effect, experiments were conducted in which increasing amounts of Ca were added to a standard Fe solution during a series of measurements. The drift-corrected ^{57}Fe/^{54}Fe was observed to increase in direct proportion to the intensity of the ^{40}Ca signal. This experiment also confirmed that, even for relatively high Ca backgrounds, the minor isotopes of Ca do not contribute significant hydrox-

ide interferences to the Fe and Cu mass regions. The hydroxide production factor for Ca, $CaOH^+/Ca^+$, is inferred to be as large as 0.2, and tends to be variable depending on source tuning conditions. We expect this relatively high CaOH production factor to be unique to cold plasma source operation. Unfortunately Ca is a ubiquitous background component and is difficult to eliminate from the analyte solutions entirely. Thus, though ^{57}Fe was measured during each analysis, the results are not reported herein.

A negative side effect of cold plasma source operation is reduction in ionization efficiency by a factor of 5 to 10. Indeed, the degree of ionization in a plasma in ionization-recombination equilibrium is expected to be a relatively sensitive function of temperature as predicted by the Saha Equation (e.g., Mermet, 1999). However, typically $\sim 5 \times 10^5$ Fe atoms were required to produced one count per second on the collector, which is about 500 times less efficient than conventional operation (desolvating nebulizer at ~1200 W RF power). The main culprit in the reduction in overall sensitivity is the nebulizer-spray chamber system, which is ~1–10% as efficient as the desolvating nebulizer. Fortunately the reduction in sensitivity is not a critical issue when making these measurements because iron is abundant in most natural samples.

All four iron isotopes were measured statically on the Axiom's multiple Faraday collector array. Potential isobaric interferences include ^{54}Cr and ^{58}Ni, which can interfere with ^{54}Fe and ^{58}Fe, respectively. The Cr content in our sample and standard solutions was negligible, although routine manual monitoring of the ^{52}Cr signal was typically performed to confirm this. The situation for Cr is also benefited by the low natural abundance of ^{54}Cr ($^{54}Cr/^{52}Cr \sim 0.03$).

Unfortunately ^{58}Ni is the most abundant Ni isotope, and ^{58}Fe is the least abundant Fe isotope ($^{58}Fe/^{56}Fe \sim 0.003$). Thus, Ni, even in small quantities can present a non-negligible isobar at ^{58}Fe. One significant source of Ni is metal hardware in the source region of the mass spectrometer. Platinum sampler and skimmer cones were used to minimize this source of background Ni. However, a Ni correction was still required for ^{58}Fe. During each data acquisition cycle, the ^{60}Ni signal was measured on an electron multiplier detector. For most analyses $^{58}Ni/^{58}Fe < 0.001$. The Ni correction required in-run cross calibration between the Axiom's axial multiplier and the Faraday counting efficiencies accurate to about 10% or better. Originally, this was accomplished by performing a secondary measurement of the $^{58}Fe/^{54}Fe$ ratio during each cycle using a Faraday-multiplier combination, with the ^{58}Fe beam measured on the multiplier. The relative gains were determined by comparing this ratio with the primary Faraday-Faraday $^{58}Fe/^{54}Fe$ measurement. Installation of a new multi-multiplier detection system on the Axiom midway through the course of this work required that this protocol be modified to reduce the beam intensities experienced by the new multiplier. Currently, cross calibration is performed by measurement of the intensity of a background molecular peak, typically FeOH, on both the axial multiplier and Faraday cups during each cycle.

2.4. Mass Discrimination Correction

Instrumental mass bias is a ubiquitous feature of mass spectrometers. Any kinetic energy-dependent process can potentially discriminate between different isotopes of an element. Often the extent of instrumental mass fractionation changes with time during a measurement. We refer to this as mass bias drift.

For ICP-MS instruments, the problem of instrumental mass bias can be exacerbated by the presence of contaminants in the analyte solution. These so-called 'matrix' elements may enhance space charge ion dispersion or shift the vaporization position of the analyte in the source plasma, thereby causing additional mass fractionation (Carlson et al., 2001). Whatever its source, the presence of this potential problem underscores the importance of high-resolution chemical separation.

2.4.1. Sample-standard bracketing

In the present work, instrumental mass bias was compensated for by sample-standard bracketing (e.g., Zhu et al., 2000) and, for some analyses, using the element Cu to monitor the instrumental mass fractionation in-run (e.g., Anbar et al., 2000; Roe et al., 2002). Sample-standard bracketing (SSB) relies on the assumption that samples and standards are mass fractionated the same way during measurement. Sample analyses are alternated between analyses of an Fe standard. Mass bias is normalized out by referencing the isotopic composition of each sample measurement to the mean composition of standards measured immediately before and immediately following the sample measurement. Typically, a single complete analysis consisted of 5 standard-sample-standard measurement cycles. The system was thoroughly washed with a 5% nitric solution between measurements. Individual measurements consisted of 3 to 5 data acquisition cycles. Each cycle included determinations of the detector baselines, Fe isotope ratios, Ni background and Faraday/multiplier cross calibration factor. Iron isotope ratios were determined by static multi-collection in 10–30 second integrations/cycle at a ^{56}Fe beam intensity of $\sim 4 \times 10^8$ counts/s (~ 6.5 V). This required an uptake rate of ~ 40 μL/min for a ~ 30 ppm Fe solution.

We chose as our standard ultra-pure iron metal purchased from the Johnson Matthey Co. (Puratronic batch Nm30597), dubbed 'P1′. P1 was sufficiently pure so that it could be analyzed without requiring additional chemical processing and purification. The isotopic composition of P1 is not accurately known. Therefore, ratios are tabulated as isotopic deviations with respect to the composition of this artificial reference material. Note that later in this paper we report data re-referenced to the mean composition of a terrestrial basalt reference sample.

For accurate mass bias correction, SSB requires that there is no differential fractionation between sample and standard due to matrix effects. This requirement can be difficult to confirm.

2.4.2. Multi-element external drift correction

In principle, these problems with SSB can be compensated for by use of an external multi-isotope standard. For Fe analyses, previous workers have used well-calibrated iron double-isotope spikes (e.g., Beard et al., 1999) or a Cu standard analyzed concurrently with Fe (Anbar et al., 2000; Sharma et al., 2001) for this purpose. The latter approach, which we refer to herein as multi-element external drift correction (MEDC), was used in the current study. For some measurements, a purified Cu standard was added to both sample and standard solutions. The Fe and Cu isotope ratios were measured successively by static multi-collection during each data acquisition cycle. Since the Cu isotope composition is the same in the sample and in the standard, this technique, in principle, provides an independent monitor of the instrumental mass fraction.

Correcting instrumental mass bias using an external (in-run) elemental standard is not straightforward. Traditionally, an empirical mathematical relationship describing the mass dependence of the instrumental mass bias, a so-called mass fractionation law, is assumed. Assumed fractionation laws are explicit functions of isotopic mass written in terms a fractionation factor, which expresses the degree of isotopic mass fractionation (e.g., Russell et al., 1978). Drift in the instrumental mass bias is expressed as a time dependence in the fractionation factor. For elements analyzed concurrently, the degree of mass fractionation (i.e., the value of the fractionation factor) for one element can in principle be used to correct the measured composition of the other element using the assumed fractionation law. However, recent experiments have shown that instrumental isotopic mass fractionation in a plasma source is element-dependent (e.g., Carlson et al., 2001). Maréchal et al. (1999), White et al. (2000), and Anbar et al. (2001) demonstrated that the ratio between fractionation factors of two elements measured simultaneously by ICP-MS is generally constant over the course of a measurement.

We assume here that the ion current 's_i' for an individual isotope 'i' at the detector side of the mass spectrometer can be expressed in the general functional form:

$$S_i = S_i\, f_n\,(m_i, t) \tag{1}$$

where 'S_i' is the ion current that would be present if there were no instrumental mass bias and 'f_n' is a function of the isotopic mass 'm_i' and time 't'. A measured isotope ratio 'r_{ji}' between isotopes 'j' and 'i' can then be written:

$$r_{ji} = \frac{S_j}{S_i} = \frac{S_j f_n(m_j, t)}{S_i f_n(m_i, t)} = R_{ji}\,\frac{f_n(m_j, t)}{f_n(m_i, t)} \tag{2}$$

where 'R_{ji}' is the true isotope ratio. In the Appendix, we show that most

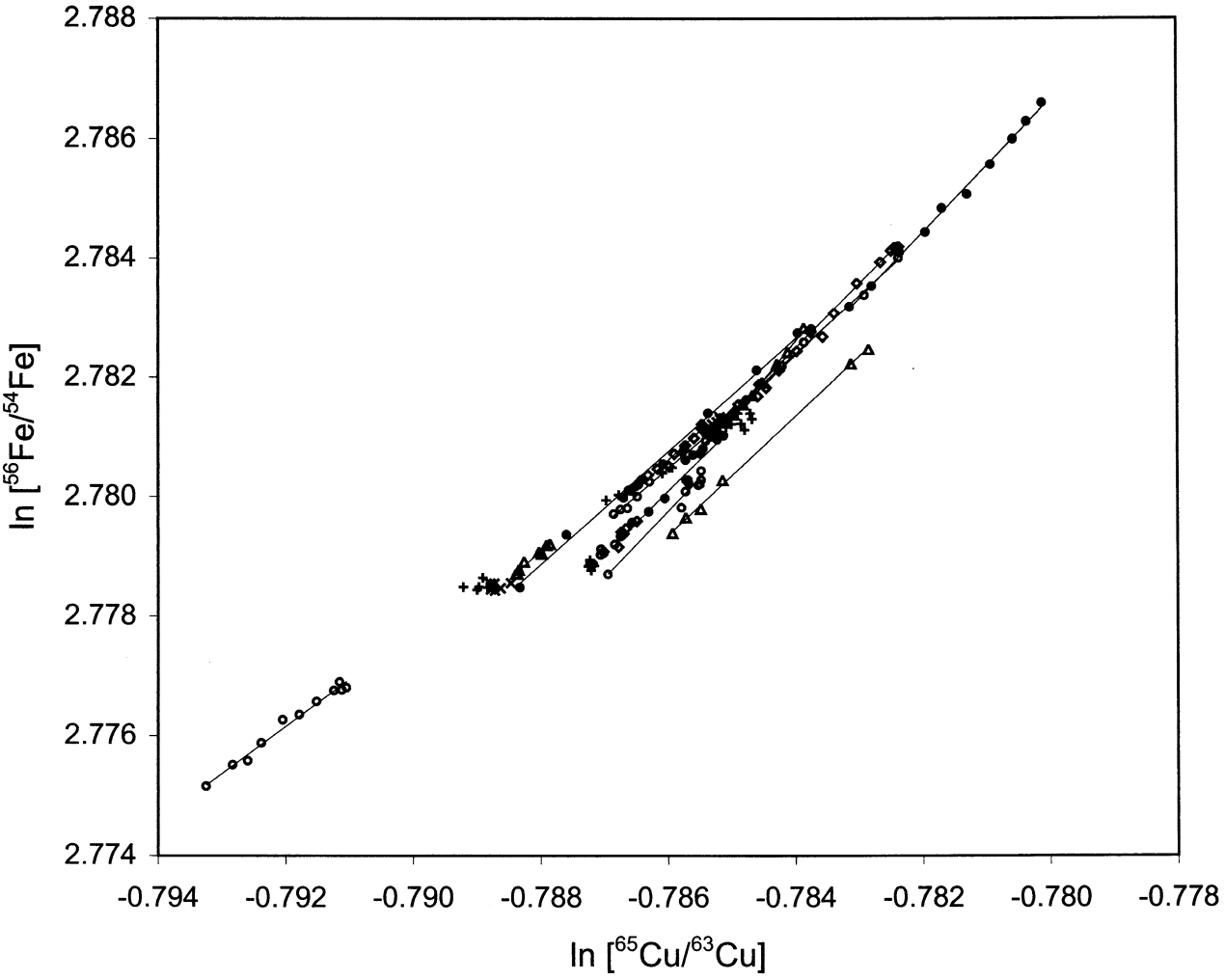

Fig. 1. Results of a series of analyses of the P1 Fe standard performed over the course of ~ 1 yr. For these experiments, P1 was doped with a Cu standard and the Fe and Cu isotopic compositions were measured during the same measurement cycle. Most of the analyses were performed on different days during different measurement sessions. The ratios are plotted in log space. According to Eqn. 6, instrumental drift will cause the ratios to plot along a straight line provided that the ratio between their fractionation factors remains constant during analysis. See text for discussion.

commonly used mass fractionation laws can be expressed using the following generalized form for f_n:

$$f_n(m_i, t) = g\int_{m_o}^{m_i} m^n dm \tag{3}$$

where 'g' is a function of time, 'n' is a constant that depends on which mass fractionation law is assumed (see Appendix), and m_o is an arbitrary reference mass. The measured isotope ratio in Eqn. 2 can then be written:

$$r_{ji} = R_{ji} g \int_{m_o}^{m_i} m^n dm - \int_{m_o}^{m_i} m^n dm = R_{ji} g \int_{m_i}^{m_j} m^n dm \tag{4}$$

Taking the logarithm of r_{ji}/R_{ji} gives

$$\ln\left[\frac{r_{ji}}{R_{ji}}\right] = I_{ji} \ln[g] \tag{5}$$

where

$$I_{ji} = \int_{m_i}^{m_j} m^n dm \tag{5b}$$

We refer to ln[g] as the generalized fractionation factor. Following the analysis of Maréchal et al. (1999), we can divide Eqn. 5 by a similar equation for a concurrently measured isotope ratio of a different element 'r_{kl}' with generalized fractionation factor ln[h], giving:

$$\ln[r_{ji}] = (\ln[r_{kl}] - \ln[R_{kl}]) \frac{I_{ji} \ln[g]}{I_{kl} \ln[h]} + \ln[R_{ji}] \tag{6}$$

If the ratio between the generalized fractionation factors, ln[g] and ln[h], remains constant throughout a measurement, a series of simultaneously measured ratios, r_{ji} and r_{kl}, should form a line on a ln-ln plot with a slope proportional to ln[g]/ln[h]. Because Eqn. 3 is a general function, this result is independent of the mass fractionation law used.

Figure 1 shows the results of a series of analyses of a mixed Fe-Cu standard measured over a one year span, with ln(^{56}Fe/^{54}Fe) plotted against ln(^{65}Cu/^{63}Cu). Data are grouped by analysis. Most analyses occurred on different days. Least squares linear fits to each data set are

Table 1. Statistics for linear fits in Fig. 1.

Run	slope	intercept	R^2	probability
P1_1	1.01 ± 0.08	3.57 ± 0.06	0.962	1.33E–03
P1_2	0.2 ± 0.3	3.0 ± 0.2	0.069	8.12E–01
P1_3	1.30 ± 0.03	3.80 ± 0.03	0.997	1.51E–04
P1_4	1.0 ± 0.1	3.54 ± 0.08	0.958	3.18E–02
P1_5	1.11 ± 0.10	3.65 ± 0.08	0.950	5.55E–04
P1_6	0.78 ± 0.03	3.40 ± 0.03	0.985	5.36E–07
P1_7	1.0 ± 0.2	3.6 ± 0.2	0.831	5.87E–02
P1_8	0.1 ± 0.2	2.9 ± 0.2	0.087	6.85E–01
P1_9	0.5 ± 0.4	3.2 ± 0.3	0.193	6.11E–01
P1_10	1.11 ± 0.02	3.65 ± 0.02	0.997	3.88E–08
P1_11	0.92 ± 0.03	3.51 ± 0.03	0.991	8.67E–06
P1_12	1.02 ± 0.07	3.58 ± 0.06	0.969	9.05E–04
P1_13	0.2 ± 0.2	2.9 ± 0.2	0.120	6.60E–01
P1_14	0.97 ± 0.02	3.54 ± 0.01	0.998	1.15E–03
P1_15	0.7 ± 0.2	3.3 ± 0.2	0.744	3.22E–01
P1_16	1.06 ± 0.05	3.62 ± 0.04	0.988	1.33E–04
P1_17	1.00 ± 0.02	3.57 ± 0.01	0.999	1.07E–03
P1_18	0.64 ± 0.06	3.28 ± 0.05	0.961	6.49E–03
P1_19	0.95 ± 0.02	3.53 ± 0.02	0.997	1.52E–04
P1_20	0.9 ± 0.2	3.5 ± 0.2	0.817	2.72E–01
P1_21	−0.4 ± 0.9	2.4 ± 0.7	0.049	7.13E–01
P1_22	1.0 ± 0.1	3.6 ± 0.1	0.941	4.40E–02
P1_23	0.91 ± 0.06	3.50 ± 0.05	0.972	7.33E–04
P1_24	1.07 ± 0.01	3.62 ± 0.01	0.999	3.33E–09

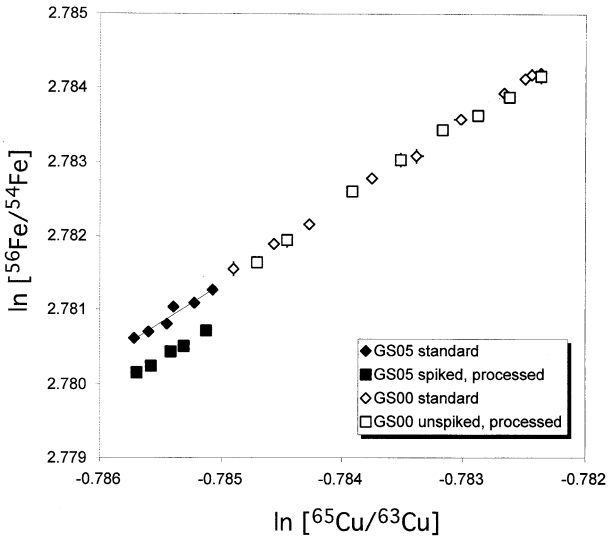

Fig. 3. Iron-Cu data from analyses of two different gravimetrically spiked aliquots of P1. Data are plotted in log space to permit delineation and correction for instrumental mass bias drift. In each analysis, a sample of P1 spiked with a monoisotopic ^{54}Fe was measured with respect to an unspiked aliquot of P1. Spiked samples were treated like normal samples and subjected to the full battery of chemical procedures before measurement. The filled symbols depict data from GS05, an analysis of a P1 sample with a gravimetrically prepared composition of $\delta^{56}Fe \cong -0.5$ ‰. This deviation is responsible for the vertical displacement between filled diamond symbols (unspiked P1) and the filled squares (spiked P1). The open symbols depict data from GS00. For this analysis, an aliquot of P1 was left unspiked ($\delta^{56}Fe = 0$ ‰), subjected to Fe separation chemistry and subsequently measured. As expected, the GS00 "standard" and "processed" sample plot along the same drift line indicating that they have identical Fe isotope compositions. These experiments helped to verify that the technique is capable of resolving subper mil Fe isotope deviations, and that the sample preparation chemistry does not induce significant Fe mass fractionation.

also shown. Table 1 gives the slope, intercept, and quality of fit statistics, expressed by the square of the linear correlation coefficient, R^2. The final column gives the probability that the same number of data points from a completely uncorrelated dataset would produce the same R^2 value (Bevington and Robinson, 1992). Most of the analyses plotted in Figure 1 display a linear trend indicating that Eqn. 3 is an adequate formulation of the instrumental mass bias for the range of observed fractionations, and that the ratio between the fractionation factors for Fe and Cu is roughly constant during each analysis. However, the ratio between the fractionation factors for Fe and Cu does change from day to day as indicated by the variable slope and intercept of the regression lines for various analyses (note that the ratio between the fractionation factors appears in the expressions for both slope and intercept in Eqn. 6). This behavior is consistent with previous observations of pairs of elements isotopically analyzed by ICP-MS: Cu-Zn (Maréchal et al., 1999), Pb-Tl (White et al., 2000), Mo-Zr and Mo-Ru (Anbar et al., 2001), Ag-Pd (Carlson and Hauri, 2001), and Fe-Cu (Roe et al., 2002). A linear fit is not appropriate for several of the data sets ($R^2 << 1$) plotted in Figure 1 (P1_2, P1_8, P1_9, P1_13, and P1_21). These cases are confined to instances where there was very little drift in the instrumental mass bias during the course of the run. To correct for instrumental mass bias drift using MEDC, standard Cu is added to both the sample and standard solutions. Sample analyses are interleaved with analyses of the standard, as in SSB. If sample and standard have the same Fe isotope composition, plots of $\ln(^{56,58}Fe/^{54}Fe)$ versus $\ln(^{65}Cu/^{63}Cu)$ should lie along the same drift line in a plot similar to Figure 1. On the other hand, if the Fe isotopic composition of the sample is significantly different from that of the standard, the sample points will be vertically displaced from the drift line of the standard (these two situations are depicted in Fig. 3, described below). The size of the displacement is a function of the difference in isotopic composition between sample and standard.

MEDC is designed to correct for drift in the instrumental mass bias and would therefore seem inappropriate when the degree of drift approaches zero. Several cases in which there was relatively little mass bias drift can be identified in Figure 1. In the absence of significant mass bias drift during an analysis, counting statistics and detector noise are mainly responsible for scatter in the measured Fe and Cu isotope ratios. Linear fits to the drift, in these cases, produce R^2 close to zero (see Table 1). Provided that sample and standard exhibit the same degree of statistical scatter and provided that the number of ratios acquired is sufficient to resolve the statistical behavior, mass bias correction by MEDC and SSB would be expected to give essentially the same result. This is because in the absence of drift, the difference between the isotopic compositions of the sample and standard becomes insensitive to the slope of the drift line. Consistent with this expectation, in each of the cases identified in Figure 1 where the degree of drift approaches zero (and R^2 tends toward zero), mass bias correction by MEDC and SSB yields the same result, within uncertainties.

2.4.3. Matrix effects

The presence of concomitant elements in the analyte solution can suppress or enhance signal intensity (Horlick and Montaser, 1998) and, in some cases, introduce isotopic mass bias (Carlson et al., 2001). For example, during MEDC analyses, the presence of Cu in the analyte solution causes matrix suppression of the Fe signal. To avert potential mass bias associated with this effect, great care was taken to match the concentration of both Cu and Fe in both sample and standard solutions.

Isotopic mass fractionation due to matrix effects can be corrected with MEDC provided the presence of a matrix species does not significantly alter the ratio between the fractionation factors of the measured elements. One trace element, Ga, behaves almost identically to Fe on the anion resin and thus was present in measurable amounts in some sample solutions. However, test solutions mixed with Ga/Fe ratios as high as 0.1—far exceeding the Ga content of any of the samples analyzed so far—did not exhibit measurable matrix-enhanced instrumental fractionation. So-called 'auto' or 'self-enhancing' matrix effects can occur when the concentrations of analyte elements in the sample and standard solutions are not matched. Jiang et al. (1988) first observed this effect in cold plasma studies of K. At relatively high analyte

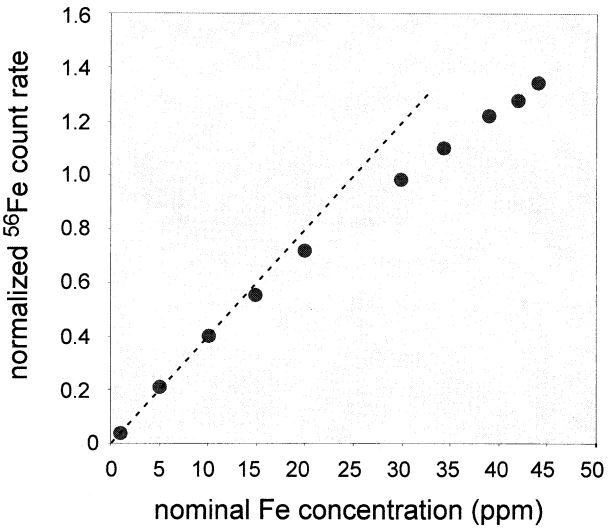

Fig. 2. Suppression of ion extraction efficiency due to iron auto-matrix effect. Iron-56 count rate is plotted versus the nominal iron concentration in the analyte solution. Count rates are normalized to the 30 ppm Fe solution. Points would fall on the dashed line if an increase in concentration yielded an equivalent increase in the ^{56}Fe signal.

concentrations, further increases in concentration did not produce a proportional increase in K^+ signal, suggesting that under these conditions, ion production becomes increasingly less efficient as the concentration of analyte (and presumably matrix) elements increases.

We observe similar behavior for Fe. Figure 2 shows the observed variation in ^{56}Fe signal as a function of concentration. A gradual decrease in the effective ionization efficiency is evident. The cause of this auto matrix suppression could be that the increased sample load enhances the electron density in the plasma, leading to an increase in the rate of electron-ion recombination, as argued by Tanner (1995). Alternatively, changes in analyte concentration could affect the rate of vaporization of sample aerosol particles in the source plasma as suggested by Olesik et al. (1999). To the extent that aerosol vaporization is controlled by plasma temperature, cold plasma operating conditions could be particularly sensitive to this effect. We have experimented with measuring standards at various concentrations to determine whether auto-matrix effects can cause isotopic mass bias. These studies have been inconclusive. In some extreme instances we have observed a $\pm$ 0.2 ‰ isotopic deviation in the measured ^{56}Fe/^{54}Fe ratio correlated with a 10% increase or decrease in the analyte concentration relative to a fixed-concentration standard for SSB (Cu-free) analyses. However this effect is not reproducible from session to session, suggesting that it may be related to specific source tunings or configurations of the sample introduction system. Moreover, for MEDC analyses, the presence of Cu in sample and standard appears to mitigate the effect. The cause of the intermittent concentration-dependent mass discrimination is not clear. We are not aware of similar observations of concentration-related mass discrimination effects for normal power (hot) Ar ICPs. Thus, it could be unique to cold plasma operation, and may indeed be related to the auto-matrix effect responsible for the decrease in ionization efficiency exhibited in Figure 2. Though we do not yet understand the cause of these effects, we acknowledge that, in principle, the accuracy of isotope ratio measurements can be compromised when analyte concentrations in sample and standard are not carefully matched, at least under cold plasma conditions. For this reason, efforts were undertaken to closely match the analyte concentrations in sample and standard. While many of the results reported in this paper were obtained using simple SSB drift correction, no results are reported in which the Fe concentrations in the sample and standard differed by more than about 5%.

Table 2. Analyses of spiked standards.

	Known Composition		Measured Composition	
	δ ^{56}Fe	δ ^{58}Fe	δ ^{56}Fe	δ ^{58}Fe
GS 00	$\equiv$ 0	$\equiv$ 0	−0.03 (4)	−0.01 (2.6)
GS 5.1	−0.49	−0.49	−0.50 (4)	−0.7 (5)
GS 5.2	−0.49	−0.49	−0.49 (7)	−0.2 (9)
GS 10.1	−0.98	−0.97	−1.07 (7)	−1.2 (3)
GS 10.2	−0.98	−0.97	−1.03 (3)	−1.2 (4)
GS 20	−1.94	−1.92	−1.93 (9)	−2.5 (4)

$\delta\ ^{i}\mathrm{Fe} = 1000 \times [(^{i}\mathrm{Fe}/^{54}\mathrm{Fe}_{\text{spiked P1}})/(^{i}\mathrm{Fe}/^{54}\mathrm{Fe}_{\mathrm{P1}}) - 1]$ where i = 56 or 58.

2.5. Analyses of Spiked Standards

To assess the accuracy of the technique, a series of gravimetrically spiked standards were prepared by mixing the P1 standard with a monoisotopic spike of ^{54}Fe (Oakridge batch 166692). Each gravimetric spike was submitted to the same dissolution and column chemistry used for sample analysis. The composition of each was then measured with respect to the unspiked P1. Figure 3 shows the results of two such analyses where mass bias was corrected using MEDC. As in Figure 1, the data are plotted in ln(^{56}Fe/^{54}Fe)-ln(^{65}Cu/^{63}Cu) space. The open symbols in Figure 3 are data taken from the analysis of GS00, an unspiked sample of P1 passed through dissolution and column chemistry. Its composition, as expected, is indistinguishable from the unprocessed standard. The filled points are data from a measurement of GS05, whose ^{56}Fe/^{54}Fe composition was gravimetrically mixed 0.5 ‰ lighter than unspiked P1. Its composition lies vertically displaced from the P1 drift line, reflecting its differing isotopic composition.

Table 2 shows the results of analyses of various spike standards. Quoted uncertainties are 2σ and represent the in-run precision of the measurement. The measured compositions are shown as deviations in parts/10^3 (delta values) from the unspiked P1 standard for both ^{58}Fe/^{54}Fe and ^{56}Fe/^{54}Fe. Agreement in Table 2 is generally excellent, with only hints of a discrepancy for the measured ^{58}Fe/^{54}Fe ratio in GS20. The results in Table 2 indicate that little mass fractionation occurs on the anion separation columns and confirms the ability to precisely resolve relatively subtle isotopic shifts with the cold plasma ICP-MS technique.

3. RESULTS

3.1. Reproducibility: Repeated Measurements of the Kil1919 Basalt Reference Sample

To assess the external precision of our iron analyses technique, repeated measurements of a terrestrial igneous rock reference sample were performed. The Hawaiian basalt Kil1919 (Rhodes, 1996) was adopted for this work. Iron was chemically separated from aliquots of a powdered Kil1919 sample and measured by cold plasma ICP-MS. Data from this series of measurements were acquired during a nine-month span, representing seven different column chemistry batches. These data are depicted on a three-isotope plot in Figure 4, where ^{56}Fe/^{54}Fe and ^{58}Fe/^{54}Fe ratios are expressed as delta value deviations from the composition of P1 on the ordinate and abscissa, respectively. The dashed line represents the array of Fe compositions that can arise from mass-dependent fractionation assuming all samples had the same starting composition. Plotted uncertainties are 1σ and represent the internal precision of each measurement. Data analyzed using SSB and MEDC are distinguished by open and closed symbols, respectively.

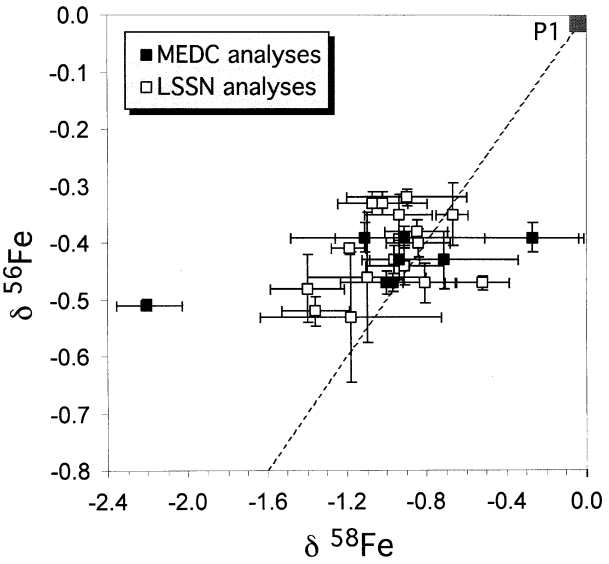

Fig. 4. Results of multiple analyses of the Kil1919 terrestrial basalt reference sample plotted on a three isotope plot. Data are reported as delta value deviations from the isotopic composition of P1: $\delta\ ^{i}Fe = 1000 \times [(^{i}Fe/^{54}FeKil_{1919})/(^{i}Fe/^{54}FeP1) - 1]$ where i = 56 or 58. Accordingly, P1 lies at the point $\delta^{56}Fe = \delta^{58}Fe = 0$ on the upper right of the plot. Samples corrected for instrumental mass bias using SSB and MEDC are identified by open and filled squares, respectively (see text for discussion). Plotted uncertainties are 1-σ, derived from internal statistics for each measurement. The dashed line delineates the array of compositions related to P1 by isotopic mass fractionation. Evident in the figure is that P1 is isotopically heavier than the Kil1919 basalt sample. The displacement in these compositions suggests that P1 experienced significant isotopic mass fractionation, presumably during an industrial purification process, or that it is derived from a reservoir with an isotopic composition distinct from the Kil1919 basalt.

The composition of P1 lies at the origin of Figure 4 on the upper right, significantly displaced from the Kil1919 average by about 0.2 ‰ amu^{-1}. A priori it is expected that rocks of igneous origin are unfractionated with respect to the average terrestrial iron composition, and indeed previous measurements tend to support this assumption (Beard and Johnson, 1999). As discussed below, the apparent mass fractionation separating P1 from Kil1919 strongly suggests that P1 is not an isotopically representative sample of terrestrial Fe. This is not surprising considering that P1 was subjected to a number of potentially low-yield, industrial purification stages during processing, any one of which may have induced isotopic mass fractionation.

Relative to the P1 standard, the error-weighted mean composition of Kil1919 is $\delta^{56}Fe = -0.428 \pm 0.008$, $\delta^{58}Fe = -0.96 \pm 0.07$ (1 sigma error in mean). Ignoring the outlying data point, the error-weighted mean is $\delta^{56}Fe = -0.411 \pm 0.009$, $\delta^{58}Fe = -0.92 \pm 0.07$. (The slightly improved uncertainty in the mean $\delta^{56}Fe$ value when the outlier is included is the result of the relatively small uncertainty associated with the outlier; in this case, inclusion of the well-constrained point reduces the uncertainty in the error-weighted mean.) These values are within two sigma of being consistent with pure mass fractionation. Ignoring the outlying point, the 1-σ standard deviations, which represent the day-to-day reproducibility of the $\delta^{56}Fe$ and $\delta^{58}Fe$ values, are 0.06 ‰ and 0.25 ‰ respectively. While no efforts were made to assess the absolute Fe composition of Kil1919 in this study, a priori it should correspond roughly to the Earth-Moon igneous average determined by Beard and Johnson (1999), who employed a double-isotope spike TIMS technique: $^{56}Fe/^{54}Fe = 15.703$ (4) and $^{58}Fe/^{54}Fe = 0.04807$ (2).

Table 3. Iron isotope ratios in various meteorites*.

Sample	Description	$\delta\ ^{56}Fe$	$\delta\ ^{58}Fe$
Allende bulk	Bulk Chondrite (CV3)	−0.06 ± 0.01	−0.05 ± 0.13
ALHA 77216	Bulk Chondrite (L3)	−0.09 ± 0.02	−0.19 ± 0.25
ALHA 77278	Bulk Chondrite (LL3)	−0.02 ± 0.06	−0.04 ± 0.25
Leoville	Bulk Chondrite (CV3)	−0.13 ± 0.06	−0.28 ± 0.25
Admire	Pallasite, silicate	−0.05 ± 0.06	−0.01 ± 0.25
Murchison	Bulk Chondrite (CM)	−0.12 ± 0.06	−0.10 ± 0.25
Orgueil	Bulk Chondrite (CI)	−0.04 ± 0.06	−0.05 ± 0.28
Grant	Iron (IIIB)	−0.05 ± 0.06	−0.33 ± 0.25
Old Woman	Iron (IIB)	−0.02 ± 0.06	0.49 ± 0.25
Canyon Diablo	Iron (IA)	−0.02 ± 0.07	−0.11 ± 0.25
Brenham	Pallasite, metal	0.04 ± 0.06	0.61 ± 0.25
Tchon1	Tieschitz Chondrule	0.00 ± 0.06	0.21 ± 0.40
Tchon2	Tieschitz Chondrule	−0.33 ± 0.02	−0.71 ± 0.15
Tchon3	Tieschitz Chondrule	−0.16 ± 0.06	−0.28 ± 0.30
Tchon4	Tieschitz Chondrule	−0.17 ± 0.06	−0.39 ± 0.25
Tchon5	Tieschitz Chondrule	−0.45 ± 0.06	−0.98 ± 0.25
Tchon6	Tieschitz Chondrule	−0.09 ± 0.06	−0.16 ± 0.25
Tchon7	Tieschitz Chondrule	−0.23 ± 0.06	−0.46 ± 0.25
Tchon8	Tieschitz Chondrule	−0.19 ± 0.06	−0.46 ± 0.25

* Compositions reported as deviations from the composition of the Kil1919 terrestrial basalt: $\delta\ ^{i}Fe = 1000 \times [(^{i}Fe/^{54}Fe_{sample})/(^{i}Fe/^{54}Fe_{Kil1919}) - 1]$ where i = 56 or 58.

3.2. Meteorite Measurements

The iron compositions of six bulk chondrites (two ordinary chondrites and four carbonaceous chondrites), three bulk irons, silicate and iron from two different pallasites and eight individual chondrules separated from an ordinary chondrite were measured by cold plasma ICP-MS. The results of these analyses are recorded in Table 3 and plotted in a three-isotope plot in Figure 5. Though all measurements were performed with P1 as a standard, for the sake of simplicity, the delta values have been re-referenced to the measured mean composition of Kil1919, our proxy for the terrestrial average Fe composition, in Figure 5 and Table 3. The quoted uncertainties are either the 1-σ external precisions derived from repeated analyses of the Kil1919 basalt, or the in-run statistical uncertainties of the measurement, whichever is larger. For a few samples, replicate measurements were performed and the calculated uncertainties are correspondingly smaller. As in Figure 4, the dashed line delineates the range of compositions that are related by mass fractionation.

4. DISCUSSION

The iron isotope compositions of the bulk chondrites, irons and pallasites all lie within two sigma of the Kil1919 basalt average. This includes the CI chondrite Orgueil for which a mass fractionated Fe composition of $\delta^{56}Fe = 0.38 \pm 0.06$ (2 sigma) relative to the IRMM-14 standard was previously reported (Zhu et al., 2001). Multiple meteorite parent bodies are represented in Figure 5. Carbonaceous chondrites have bulk

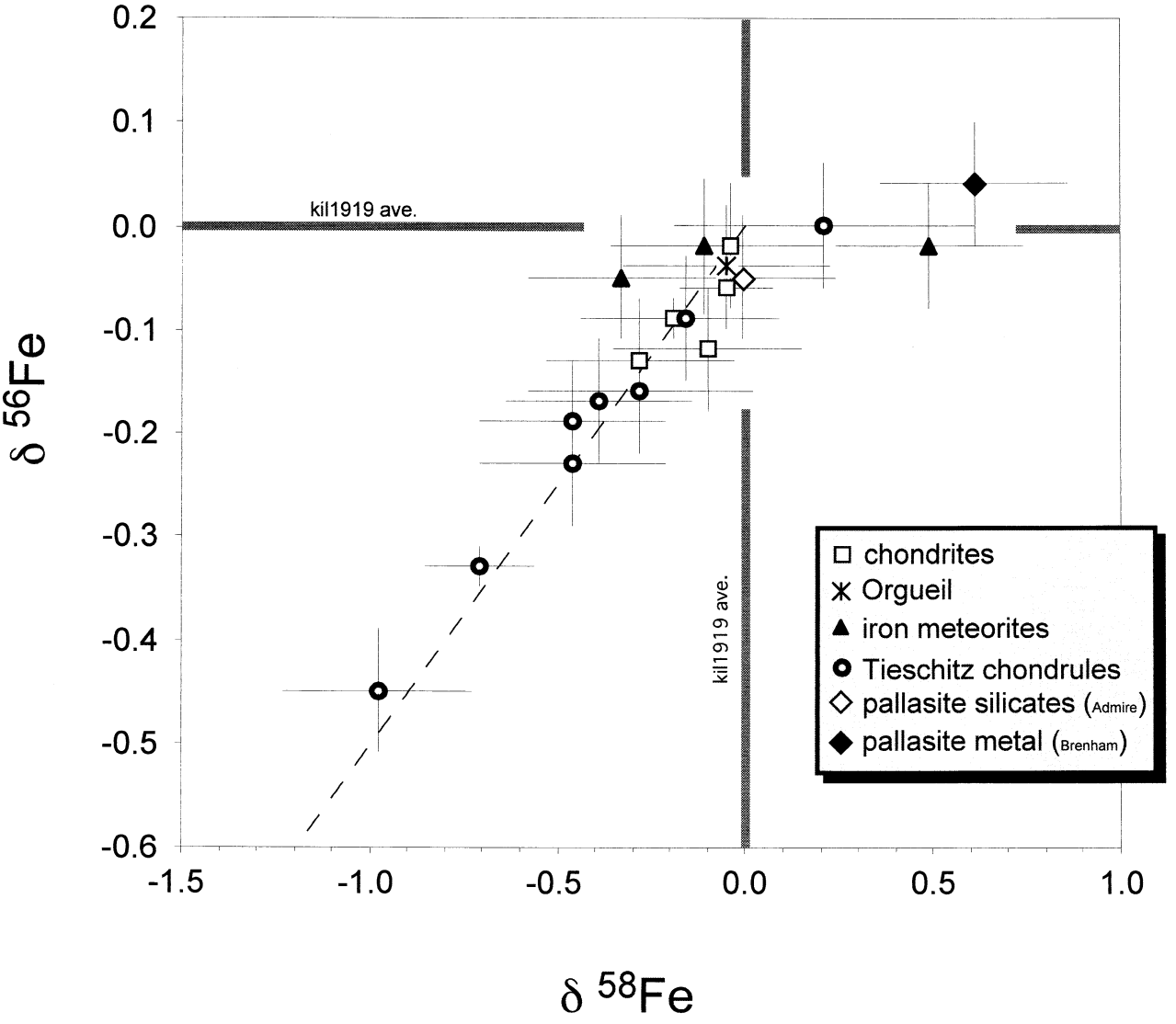

Fig. 5. Three isotope plot of Fe isotope compositions of several bulk meteorites and suite of ordinary chondrite chondrules. Data are taken from Table 3. Plotted values have been re-referenced to the mean composition of the Kil1919, a proxy for the terrestrial average. Plotted error bars are 1-σ external uncertainties. The bulk meteorites, including the primitive carbonaceous chondrite Orgueil, have compositions identical, within error, of the terrestrial basalt. The ordinary chondrite chondrules have compositions consistent with mass fractionated chondritic Fe.

chemical compositions similar to the solar photosphere and are probably derived from undifferentiated parent bodies that formed in the solar nebula (Anders, 1971). Irons and pallasites are from parent objects that experienced metal-silicate differentiation. The data in Figure 5 include both magmatic (IIB, IIIB) and non-magmatic irons (IA), the former presumably representing core material from a differentiated asteroid. On the other hand, the Kil1919 Hawaiian basalt samples iron from the Hawaiian mantle plume. Similarity between the iron isotope ratios from these diverse sources suggests that there was no significant large-scale iron isotope fractionation in the solar nebula.

As shown in Figure 5 and Table 3, data from one of the iron meteorites (Old Woman-IIB) and metal from one pallasite (Brenham) plot more than 1-σ from the mass fractionation line. However, the 2-σ error ellipses for both of these points overlap the mass fractionation line. That both plot with apparent ^{58}Fe enrichments is probably fortuitous; a careful examination of the raw data from those runs revealed no evidence of systematic effects that could explain the apparent shift. It should be noted that such effects are not unexpected for a data set of this size, assuming that there are no isotopic anomalies present (this assumption is consistent with the results of Zhu et al., 2001). It is therefore argued that the apparent divergence of these data from the mass fractionation line does not constitute evidence for a ^{58}Fe-enriched composition in these meteorites. Confirmation of this conclusion awaits repeated analyses.

There are some apparent inconsistencies between these results and those of Zhu et al. (2001), who observed variable Fe isotopic fractionation among bulk meteorite samples, especially

for undifferentiated meteorites. Though not pointed out in their paper, among measurements of materials from chondrites, Zhu et al. (2001) observed isotopically heavy Fe in fractions that presumably experienced more aqueous alteration, such as the matrices of Allende and Chainpur (LL3), and Orgueil whole rock. Their results appear to fit with a scenario in which aqueous activity led to heavy isotope enrichments in altered phases, perhaps by equilibrium isotope partitioning between Fe(II)- Fe(III)-bearing compounds (Polyakov, 1997; Schauble et al., 2001). Without measurements of separated chondrite matrices, we are unable to corroborate this result. Some assessment of the degree of aqueous alteration, especially in studied chondrules (see below), would be valuable in future Fe isotope studies of meteorites.

The reason for the difference in the results for Orgueil between the two labs remains unclear and bears further study. The Zhu et al. (2001) measurements show Orgueil to be fractionated by about 0.4 ‰ from their terrestrial standard (IRMM-14 reference Fe) for δ^{56}Fe, whereas our analysis of Orgueil shows it to have a composition identical to Kil1919, within uncertainties. It is unlikely that this is due to differences between the compositions of Kil1919 and the IRMM-14 reference standard. For one thing, if the composition of IRMM-14 differed significantly from chondritic or from igneously processed terrestrial Fe, a systematic offset in the delta value deviations would have been detected. Also, Zhu et al. measured nearly identical iron isotopic compositions for bulk Allende and Murchison, which were indistinguishable within uncertainties from the composition of the IRMM-14 standard. Likewise, we measure identical compositions for Kil1919, Allende bulk and Murchison bulk.

As one reviewer points out, Orgueil is known to be chemically and mineralogically heterogeneous on the $\leq$ 100 μm scale (Endreβ and Bischoff, 1996; Morlok et al., 2001). Moreover, the carbonaceous chondrites, particularly Orgueil, have been heavily altered by parent body fluids (e.g., Zolensky and McSween, 1988), and in addition, Orgueil shows evidence of having interacted with terrestrial hygroscopic water absorbed since its fall in 1864 (Gounelle and Zolensky, 2001). Isotopic heterogeneity is also apparent in Orgueil; various minerals within Orgueil appear to be in disequilibrium with respect to oxygen isotopes (e.g., Rowe et al., 1994). Thus, it is conceivable that the different Fe isotope compositions measured by the two labs could be a sampling effect. The Orgueil sample analyzed in the present work was generously supplied by Ghislaine Crozaz and Robert Walker at Washington University and consisted of several fragments 1–5 mm in size totaling 10 mg in mass. The relatively large size of the sample dissolved in the present work, and the similarity between its Fe isotopic composition and those of the irons, pallasites and other chondrites suggests that our results are reflective of the Orgueil average.

Assuming that Kil1919 is a reasonable proxy for the bulk terrestrial iron isotopic composition, and if Orgueil is similarly a reasonable representative of the primitive iron composition in the solar nebula, it can be concluded from our results that the bulk ^{56}Fe/^{54}Fe for the Earth is identical to the chondritic value to within about a part in ten thousand. Similarity between these reservoirs and those of the magmatic and non-magmatic irons suggests that planetary differentiation does not significantly fractionate iron isotopes. This conclusion is consistent with the work of Beard and Johnson (1999) and Sharma et al. (2001) who observed isotopically identical iron in igneous samples from the Earth and moon, and the Earth and the Canyon Diablo iron meteorite, respectively.

Measurements of individual chondrules extracted from Tieschitz, an unequilibrated ordinary chondrite (H3.6), reveal a tendency toward isotopically light compositions (Fig. 5). The most fractionated Tieschitz chondrule in Figure 5 has δ^{56}Fe $\sim$ -0.5 ‰, referenced to Kil1919 basalt. Previously Alexander and Wang (2001) determined that δ^{57}Fe in chondrules from another unequilibrated ordinary chondrite, Chainpur (LL3.4), are normal to within their measurement uncertainty ($\sim$ 1–2 ‰) using an ion microprobe. However, cold plasma ICP-MS offers a considerable improvement in precision over the ion microprobe technique, permitting the resolution of isotopic fine structure in Tieschitz.

Iron isotopic fractionation between matrix and chondrules in Allende (CV3) and Chainpur (LL3) were detected by Zhu et al. (2001) using ICP mass spectrometry. Similarly, Mullane et al. (2001) reported isotopic variability among Allende chondrules. In contrast to the Zhu et al. results, which show both positive and negative mass fractionation in chondrules from Allende, our results for Tieschitz show a single trend toward isotopically lighter compositions. This may suggest that the mechanism(s) for fractionation is different in these two meteorites. It is possible that iron fractionation in Tieschitz chondrules occurred as a result of a single stage process.

It is widely assumed that chondrules formed by the melting of precursor material in the solar nebula (e.g., Taylor et al., 1983), although competing models are still under discussion (Boss, 1996). A key question is whether the iron compositions observed in Tieschitz chondrules are related to the chondrule formation process or evolved subsequently as a result of parent body alteration. Previous analyses of isotope systematics in Tieschitz chondrules provide no clear answer on this point. Mass fractionated Mg isotopes (δ^{26}Mg ranging from $\sim$ -2 to $+1$ ‰) were observed in individual Tieschitz chondrules by Alexander et al. (1998). It was assumed that these compositions were produced by kinetic effects during evaporation and/or condensation in the solar nebula, or were inherited from processed chondrule precursor material. However, Ash et al. (1998) observed no significant isotopic mass fractionation of oxygen in Tieschitz chondrules, but did see tentative evidence of isotopic exchange between chondrules and ^{18}O-rich fluids on the ordinary chondrite parent body. Parent body isotope redistribution was previously inferred from radioisotope studies. I-Xe ages for ordinary chondrite chondrules (including Tieschitz) span a range of $\sim$ 50 Ma, often postdating the expected end of chondrule formation by tens of millions of years (Nichols et al., 1991; Swindle et al., 1991a; Swindle et al., 1991b; Swindle, 1998; Gilmour et al., 2000). These results and the highly variable I/Xe ratios in the chondrules imply resetting of the I-Xe system by parent body alteration (Swindle, 1998). Even later isotopic redistribution in Tieschitz is indicated by Sm-Nd and Ar-Ar measurements. Krestina et al. (1996) observed a bimodal distribution of Sm-Nd ages among Tieschitz chondrules. One subset had formation ages of 4.55 Ga, while other chondrules yielded ages of $\sim$ 2 Ga. Ar-Ar studies of bulk Tieschitz during stepwise Ar extraction show a high-tempera-

ture Ar release plateau with a low apparent age (~ 2 Ga) (Turner et al., 1978). In light of the Sm-Nd chondrule ages, Hutchison et al. (1998) recently interpreted the Ar-Ar results as evidence of aqueous alteration at ~ 2 Ga. A disturbance at 2 Ga could be indicative of an impact on the Tieschitz parent body, although Tieschitz does not appear to have been heavily shocked (Kallemeyn et al., 1989). Nonetheless, there is textural and chemical evidence of secondary aqueous alteration in Tieschitz chondrules (Hutchison et al., 1998). Chemical exchange, for example, between chondrules and matrix or rim material under such conditions can lead to isotopic mass fractionation. This is a plausible explanation for the observed range of iron isotopic compositions observed in Tieschitz. Complementary chemical and petrographic characterization would be required to address this possibility.

Assuming chondrules formed in the solar nebula by flash heating, it is also possible to explain iron mass fractionation in Tieschitz chondrules by evoking kinetic effects associated with partial evaporation of precursor solids and/or recondensation. Evaporation of chondrule precursors under Rayleigh conditions (open system evaporation with an isotopically well-mixed liquid melt) tends to enrich heavy isotopes in the residual liquid as lighter isotopes preferentially enter the gas phase. The lack of positive mass fractionation of Tieschitz chondrules suggests that either (1) evaporative loss of iron was not significant, (2) Rayleigh conditions were not met during evaporation, (3) the record of evaporative mass fractionation was erased by subsequent isotopic re-equilibration between the melt reservoir and the gas in the nebula, or (4) the record of evaporative fractionation was erased by parent body alterations. Alexander and Wang (2001) tried to explain the lack of observable positive mass fractionation of iron in Chainpur chondrules in the context of the variable FeO concentrations in chondrules. They interpreted their data as evidence that either iron evaporation was suppressed due to rapid cooling following flash heating, or that significant iron evaporation did occur, but the associated Rayleigh fractionation was subsequently erased during back reactions between the molten chondrule and the nebular gas. The latter was previously suggested as a mechanism for erasing evaporation-induced mass fractionation of K in chondrules from the ordinary chondrites Semarkona (Alexander and Grossman, 2000) and Bishunpur (Alexander et al., 2000), and would appear to require a relatively high partial pressure of isotopically normal iron in the gas. Similarly Galy et al. (2000) evoked high ambient gas pressures ($P > 100$ Pa) in the chondrule-forming region of the solar nebula to explain observed correlations between chondrule size and Mg/Al ratios, and $^{25}Mg/^{24}Mg$ ratios. Our data are qualitatively consistent with these scenarios, but offer no additional constraints on the evaporation modeling other than providing more strict upper limits that rule out preserved evaporative mass fractionation in Tieschitz chondrules.

According to the kinetic theory of gases, condensation can, in principle, cause isotopic mass fractionation when lighter isotopes preferentially enter the condensate. This occurs because, in a sufficiently diffuse gas, the molecular deposition rate over some arbitrary area is proportional to the mean thermal velocity, which is a function of $M^{-1/2}$. Fractionation is preserved provided that the condensate does not maintain equilibrium with the gas during condensation and does not subsequently diffusively re-equilibrate with the gas. Such conditions could be the result of flash heating followed by high cooling rates, where condensates form rapidly from a large, well-mixed, super cooled gas reservoir. In this case, condensation of Fe atoms or FeO could produce δ^{56}Fe values as large as -10 to -20 ‰ (assuming deposition rates proportional to $M^{-1/2}$), a range that is consistent with the chondrule compositions we measured in Tieschitz. If correct, it implies that the chondrules record the final condensation event before incorporation onto the Tieschitz parent body.

A final possibility is that the range of compositions in the Tieschitz chondrules simply reflects isotopic heterogeneity in the precursor materials. Mullane et al. (2001) recently suggested this mechanism to explain the apparent correlation between the degree of iron isotopic mass fractionation and FeO content in Allende chondrules. In this case, the lack of evidence of positive mass fractionation in the Tieschitz chondrules may reflect the fact that condensation reactions, rather than partial evaporation, play a more prominent rule in fixing the isotopic composition of the Tieschitz chondrules as they are recycled in the nebula. Alternatively, Tieschitz chondrules may have condensed from a gas with an isotopically fractionated composition. Establishing a fractionated gas reservoir could be achieved by partial evaporation of chondritic material in a flash-heating event; Rayleigh fractionation during partial evaporation would enrich the local gas reservoir in light Fe isotopes. Gas-solid separation, plausibly resulting from poor dynamical coupling between the gas flow and the solids, would separate the two components before significant re-equilibration. In the absence of the original solids, the cooling gas would condense a new generation of solids with a composition reflecting that of the isotopically light gas. Such a scenario would require the existence of a complementary reservoir of material with positive δ^{56}Fe. Our observations reveal no such heterogeneities among bulk meteorites, which means that if such a process occurred at all, it was not important for establishing the bulk iron compositions of the meteorite parent bodies. However it is interesting to note that Zhu et al. (2001) observed some degree of isotopic complementarity between the iron compositions of chondrules and matrix from Allende and Chainpur. Determining the possible relationship between the iron compositions of chondrules and matrix material in Tieschitz is one of the focuses of our ongoing investigations.

5. SUMMARY AND CONCLUSIONS

We have developed a technique for precisely measuring the isotopic composition of iron using cold plasma multi-collector inductively coupled plasma mass spectrometry. Reduced power plasma operation helps to eliminate pervasive molecular interferences from Ar complexes associated with conventional ICP-MS. Mass bias corrections are achieved by either sample standard bracketing, or external mass bias drift correction using a Cu standard analyzed simultaneously with the Fe. The external reproducibility, as indicated by repeated measurements of a terrestrial basalt reference sample, is $\pm$ 0.06 ‰ for δ^{56}Fe and $\pm$ 0.25 ‰ for δ^{58}Fe (1 σ).

Using the cold plasma technique, the iron compositions of six bulk chondrites (two ordinary chondrites and four carbonaceous chondrites), three bulk irons, silicate and iron separated

from two different pallasites and eight individual chondrules separated from an ordinary chondrite were analyzed. We observe no significant variability in the iron isotope compositions of the bulk meteorites; all have compositions within two sigma of the Hawaiian basalt reference sample. This observation suggests that large-scale mass fractionation mechanisms for iron were non-existent in the solar nebula. Furthermore, similarity between the differentiated meteorites, chondrites and the terrestrial basalt indicates that physical and chemical differentiation of planetesimals does not significantly alter the isotopic composition of iron.

Isotopically light compositions were measured in eight chondrules from the unequilibrated ordinary chondrite Tieschitz (-0.5 ‰ $< \delta^{56}Fe_{chondrules} < 0.0$ ‰). Mechanisms for producing the mass fractionated compositions in these chondrules probably operated on a local scale and could include kinetic effects in the nebula during chondrule processing or chemical fractionation on the meteorite parent body during secondary alteration. Alternatively, Tieschitz chondrules may reflect isotopic heterogeneity in the chondrule precursor material that was not entirely erased by nebular and subsequent parent body processing.

The large abundance of chondrules in primitive chondrites indicates that the chondrule-forming event was an important process that may be central to understanding the evolution of the nebula. However, the mechanism responsible for forming chondrules in the early solar system continues to evade theorists. In this effort, isotopic measurements help to constrain various models for chondrule formation and processing. The behavior of iron is particularly important in that it is the most volatile of the major elements in chondrules. Our continuing research will include studies of iron variations that occur in chondrules and other internal components in Tieschitz as well as other chondritic meteorites. One focus will be determining whether iron variations correlate with indicators of parent body alteration such as the presence of secondary phases in chondrules. Also important in this effort will be quantifying the behavior of other elements with differing volatilities and chemical properties. Different elements will vary in their response to kinetic mass fractionation conditions and the combined data set may harbor clues that will enable us to pinpoint the physical and chemical conditions in which chondrules formed.

Acknowledgments—Mary Horan and Tim Mock cheerfully assisted with many aspects of the chemistry and mass spectrometry, and we are thankful for their help. We are also indebted to Ghislaine Crozaz, Bob Walker and Tim McCoy for providing samples for this study. Thoughtful discussions with Ariel Anbar, Brian Beard, Clark Johnson, Aaron Pietruszka, Scott Tanner, and Ed Young were helpful in fostering the development of many aspects of this project. We are thankful for their input. Suggestions by reviewers Anbar, Young, Ott and one anonymous reviewer greatly improved the final version of this paper. This work was support in part by the NASA Astrobiology Institute (NCC2-1056).

Associate editor: U. Ott

REFERENCES

Alexander C. M. O'D. and Grossman J. N. (2000) The K isotopes in Semarkona chondrules (abstract). *Lunar Planet. Sci. XXXI.* Lunar Planet. Inst., Houston. #1850 (abstr.).

Alexander C. M. O'D. and Wang J. (2001) Iron isotopes in chondrules: implications for the role of evaporation during chondrule formation. *Meteorit. Planet. Sci.* **36,** 419–428.

Alexander C. M. O'D., Mock T., and Carlson R. (1998) Magnesium-isotopic fractionation in Tieschitz chondrules. *Meteorit. Planet. Sci.* **33,** A9 (abstr.).

Alexander C. M. O'D., Grossman J. N., Wang J., Zanda B., Bourot-Denise M., and Hewins R. H. (2000) The lack of potassium-isotopic fractionation in Bishunpur chondrules. *Meteorit. Planet. Sci.* **35,** 859–868.

Anbar A. D., Roe J. E., Barling J., and Nealson K. H. (2000) Nonbiological fractionation of iron isotopes. *Science* **288,** 126–128.

Anbar A. D., Knab K. A., and Barling J. (2001) Precise determination of mass-dependent variations in the isotopic composition of Molybdenum using MC-ICPMS. *Anal. Chem.* **73,** 1425–1431.

Anders E. (1971) Meteorites and the early solar system. *Ann. Rev. Astron. Astrophys.* **9,** 1–34.

Ash R. D., Rumble D. III, Alexander C. M. O'D., MacPherson G. J. (1998) Oxygen isotopes in isolated chondrules from the Tieschitz ordinary chondrite; initial compositions and differential parent body alteration. *Lunar. Planet. Sci. XXIX*. Lunar Planet. Inst., Houston. #1854(abstr.).

Beard B. L. and Johnson C. M. (1999) High precision iron isotope measurements of terrestrial and lunar materials. *Geochim. Cosmochim. Acta* **63,** 1653–1660.

Beard B. L., Johnson C. M., Cox L., Sun H., Nealson K. H., and Aguilar C. (1999) Iron isotope biosignatures. *Science* **285,** 1889–1892.

Bevington P. R. and Robinson D. K. (1992) Data Reduction and Error Analysis for the Physical Sciences, McGraw-Hill, Inc., New York. pp. 199–200.

Bigeleisen J. (1965) Chemistry of Isotopes. *Science* **147,** 463–471.

Boss A. P. (1996) A Concise Guide to Chondrule Formation Models. In *Chondrules and the Protoplanetary Disk* (eds. R. Hewins, R. Jones, and E. Scott), pp. 257–263. Cambridge: Cambridge University Press, Cambridge.

Carlson R. W. and Hauri E. H. (2001) Extending the ^{107}Pd-^{107}Ag chronometer to low Pd/Ag meteorites with multicollector plasma-ionization mass spectrometry. *Geochim. Cosmochim Acta* **65,** 1839–1848.

Carlson R. W., Hauri E. H., and Alexander C. M. O'D. (2001) Matrix-induced isotopic mass fractionation in the ICP-MS. In *Plasma Source Mass Spectrometry: The New Millennium* (eds. G. Holand and S. D. Tanner), pp. 288–297. The Royal Society of Chemistry, Cambridge, UK.

Douglas D. J. and Tanner S. D. (1998) Fundamental considerations in ICPMS. In *Inductively Coupled Plasma Mass Spectrometry* (ed. A. Montaser), pp. 615–679. Wiley-VCH, New York.

Endreβ M. and Bischoff A. (1996) Carbonates in CI chondrites: clues to parent body evolution. *Geochim. Cosmochim. Acta* **60,** 489–507.

Galy A., Young E. D., Ash R. D., and O'Nions R. K. (2000) The formation of chondrules at high gas pressures in the solar nebula. *Science* **290,** 1751–1753.

Gilmour J. D., Whitby J. A., Turner G., Bridges J. C., and Hutchison R. (2000) The iodine-xenon system in clasts and chondrules from ordinary chondrites: Implications for early solar system chronology. *Meteorit. Planet. Sci.* **35,** 445–455.

Gounelle M. and Zolensky M. E. (2001) A terrestrial origin for sulfate veins in CI1 chondrites. *Meteorit. Planet. Sci.* **36,** 1321–1329.

Horlick G. and Montaser A. (1998) Analytical characteristics of ICPMS. In *Inductively Coupled Plasma Mass Spectrometry* (ed. A. Montaser), pp. 503–588. Wiley-VCH, New York.

Hutchison R., Alexander C. M. O'D., and Bridges J. C. (1998) Elemental redistribution in Tieschitz and the origin of white matrix. *Meteorit. Planet. Sci.* **33,** 1169–1179.

Jiang S.-J., Houk R. S., and Stevens M. A. (1988) Alleviation of overlap interferences for determination of potassium isotope ratios by inductively coupled plasma mass spectrometry. *Anal. Chem.* **60,** 1217–1221.

Johnson C. M. and Beard B. L. (1999) Correction of instrumentally produced mass fractionation during isotopic analysis of Fe by thermal ionization mass spectrometry. *Int. J. Mass. Spec.* **193,** 87–99.

Johnson C. M., Skulan J. L., Beard B. L., Sun H., Nealson K. H., and Braterman P. S. (2002) Isotopic fractionation between Fe(III) and Fe(II) in aqueous solutions. *Earth Planet. Sci. Lett.* **195,** 141–153.

Kallemeyn G. W., Rubin A. E., Wang D., and Wasson J. T. (1989) Ordinary chondrites: Bulk compositions, classification, lithophile-element fractionations, and composition-petrographic type relationships. *Geochim. Cosmochim. Acta* **53,** 2747–2767.

Kehm K., Alexander C. M. O'D., and Hauri E. H. (2001a) High precision iron isotope measurements by multi-collector ICP-MS. *Lunar Planet. Sci. XXXII.* Lunar Planet. Inst., Houston. #1932 (abstr.).

Kehm K. and Hauri E. H. (2001b) Precise iron isotope measurements using cold plasma ICP-MS. *Eleventh Ann. V. M. Goldschmidt Conf.* Lunar Planet. Inst., Houston. #3580 (abstr.).

Kehm K., Alexander C. M. O'D., and Hauri E. H. (2001c) Iron isotope measurements of meteorites. *Meteorit. Planet. Sci.* **36,** A94–A95 (abstr.).

Krestina N., Jagoutz E., and Kurat G. (1996) Sm-Nd system in single chondrules from Tieschitz (H3). *Lunar Planet. Sci. XXVII.* Lunar Planet. Sci., Houston., 701–702(abstr.).

Luck J. M., Ben Othman D., Albarède F., and Barrat J. A. (2001) Cu and. Zn isotopic variations in carbonaceous chondrites and iron meteorites. *Meteorit. Planet. Sci.* **36(suppl), A118** (abstr.).

Mandernack K. W., Bazylinski D. A., Shanks W. C. III, and Bullen T. D. (1999) Oxygen and iron isotope studies of magnetite produced by magnetotactic bacteria. *Science* **285,** 1892–1896.

Maréchal C. N., Télouk P., and Albarède F. (1999) Precise analysis of cupper and zinc isotopic compositions by plasma-source mass spectrometry. *Chem. Geol.* **156,** 251–273.

Mermet J. M. (1999) Fundamental principles of inductively coupled plasmas. In *Inductively Coupled Plasma Spectrometry and its Applications* (ed. S. J. Hill), pp. 35–70. Sheffield Academic Press, Sheffield, England.

Morlok A., Bischoff A., Henkel T., Rost D., Stephan T. and Jessberger E. K. (2001) The chemical heterogeneity of CI chondrites. *Lunar Planet. Sci. XXXII.* Lunar Planet. Inst., Houston. #1530 (abstr.).

Mullane E., Russell S. S., Weiss D., Mason T. F. D., and Gounelle M. (2001) High precision iron isotope compositions in components from the Allende CV3 meteorite by MC-ICP-MS. *Eos.* **82,** F1296 (abstr.).

Nichols R. H. Jr., Hagee B. E., Hohenberg C. M. (1991) Tieschitz chondrules: I-Xe systematics. *Lunar Planet. Sci. XXII.* Lunar Planet. Inst., Houston., 975–976(abstr.).

Olesik J. W., Stewart I. I., Hartshome J. A., and Hensman C. E. (1999) Sensitivity and matrix effects in ICP-MS: Aerosol processing, ion production and ion transport. In *Plasma Source Mass Spectrometry: Developments and Applications* (eds. G. P. Holland and S. D. Tanner), pp. 3–19. Royal Society of Chemistry, Cambridge.

Polyakov V. B. (1997) Equilibrium fractionation of the iron isotopes: Estimation from Mössbauer spectroscopy data. *Geochim. Cosmochim. Acta* **61,** 4213–4217.

Rhodes J. M. (1996) Geochemical stratigraphy of lava flows sampled by the Hawaii scientific drilling project. *J. Geophys. Res.* **101,** 11729–11746.

Roe J. E., Anbar A. D., Barling J. (2003) Nonbiological fractionation of Fe isotopes: evidence of an equilibrium isotope effect. *Chem. Geol.* **195**, 69–85.

Rowe M. W., Clayton R. N., and Mayeda T. K. (1994) Oxygen isotopes in separated components of CI and CM meteorites. *Geochim. Cosmochim. Acta* **58,** 5341–5347.

Russell W. A., Papanastassiou D. A., and Tombrello T. A. (1978) Ca isotope fractionation on the Earth and other solar system materials. *Geochim Cosmochim. Acta* **42,** 1075–1090.

Schauble E. A., Rossman G. R., and Taylor H. P. Jr. (2001) Theoretical estimates of equilibrium Fe-isotope fractionations from vibrational spectroscopy. *Geochim. Cosmochim. Acta* **65,** 2487–2497.

Sharma M., Polizzotto M., and Anbar A. D. (2001) Iron isotopes in hot springs along the Juan de Fuca Ridge. *Earth Planet. Sci. Lett.* **194,** 39–51.

Strelow F. W. E. (1980) Improved separation of iron from copper and other elements by anion-exchange chromatography on a 4% cross-linked resin with high concentrations of hydrochloric acid. *Talanta.* **27,** 727–732.

Swindle T. D., Caffee M. W., Hohenberg C. M., Lindstrom M. M., and Taylor G. J. (1991a) Iodine-xenon studies of petrographically and chemically characterized Chainpur chondrules. *Geochim. Cosmochim. Acta* **55,** 861–880.

Swindle T. D., Grossman J. N., Olinger C. T., and Garrison D. H. (1991b) Iodine-xenon, chemical, and petrographic studies of Semarkona chondrules; evidence for the timing of aqueous alteration. *Geochim. Cosmochim. Acta* **55,** 3723–3734.

Swindle T. D. (1998) Implications of iodine-xenon studies for the timing and location of secondary alteration. *Meteorit. Planet. Sci.* **33,** 1147–1155.

Tanner S. D. (1995) Characterization of ionization and matrix suppression in inductively coupled 'cold' plasma mass spectrometry. *J. Anal. Atom. Spec.* **10,** 905–919.

Taylor G. J., Scott E. R. D., and Keil K. (1983) Cosmic setting for chondrule formation. In *Chondrules and their Origins* (ed. E. A. King), Lunar and Planetary Institute, Houston, TX. pp. 262–278.

Turner G., Enright M. C., and Cadogan P. H. (1978) The early history of chondrite parent bodies inferred from ^{40}Ar-^{39}Ar ages. *Proc. Lunar Sci. Conf. 9th, Geochim. Cosmochim. Acta (Suppl.)* **10,** 989–1025.

Van der Walt, Strelow F. W. E., and Verheij R. (1985) Influence of crosslinkage on the distribution coefficients and anion exchange behaviour of some elements in hydrochloric acid. *Solv. Extrac. Ion Exch.* **3(5),** 723–740.

Völkening J. and Papanastassiou D. A. (1989) Iron isotope anomalies. *Astrophys. J. Lett.* **347,** L43–L46.

Walder A. J., Platzner I., and Freedman P. A. (1993) Isotope ratio measurement of lead, neodymium, and neodymium-samarium mixtures, hafnium and hafnium-lutetium mixtures with a double focusing multiple collector inductively coupled plasma mass spectrometer. *J. Anal. Atom. Spectrom.* **8,** 19–23.

Weyer S., Schwieters J., Hamester M., Jung G., Pesch R., and Rottmann L. (2001) MC-ICPMS–High Resolution Isotope Ratio Measurements of Fe and Ca. *Eleventh Ann. V. M. Goldschmidt Conf.* Lunar Planet. Inst., Houston. #3523 (abstr.).

White W. M., Albarède F., and Télouk P. (2000) High-precision analysis of Pb isotope ratios by multi-collector ICP-MS. *Chem. Geol.* **167,** 257–270.

Zhu X. K., O'Nions R. K., Guo Y., and Reynolds B. C. (2000) Secular variation of iron isotopes in North Atlantic deep water. *Science* **287,** 2000–2002.

Zhu X. K., Guo Y., O'Nions R. K., Young E. D., and Ash R. D. (2001) Isotopic homogeneity of iron in the early solar nebula. *Nature* **412,** 311–313.

Zolensky M. and McSween H. Y. Jr. (1988) Aqueous alteration. In *Meteorites and the Early Solar System* (eds. J. F. Kerridge and M. S. Matthews), pp. 114–143. The University of Arizona Press, Tucson, AZ.

APPENDIX

The purpose of the present discussion is to justify the use of Eqn. 4 as a general mass fractionation law. Together, Eqn. 1 and (3) state that the measured ion intensity of an isotope, s_i, is related to the true intensity, S_i, by the following equation:

$$S_i = S_i g(t)^{\int_{m_o}^{m_i} m^n\,dm} \tag{AP1}$$

The integral in the exponent depends on 'n', which is an adjustable parameter that usually takes on integer values $-2 \le n \le 0$ as described below. The time dependence of g represents instrumental mass bias drift. Two simultaneously measured isotopes of mass m_i and m_j then give the expression in Eqn. 4:

$$r_{ji} = R_{ji} g^{\int_{m_i}^{m_j} m^n dm} \tag{AP2}$$

where r_{ji} and R_{ji} are the measured and true isotope abundance ratios, respectively, for isotopes j and i.

Eqn. 4 reduces to commonly-used mass fractionation laws for specific values of n. For example, setting $n = 0$ gives

$$r_{ji} = R_{ji} g^{m_j - m_i} = R_{ji} g^{\Delta m} \quad \text{(A1)}$$

This is the so-called power law as expressed by Russell et al. (1978). A first order Taylor expansion of Eqn. A1 gives $r_{ji} \approx R_{ji}$ (1 - constant $\times \Delta m$), which is the linear fractionation law. Setting $n = -1$ in Eqn. 4 gives

$$r_{ji} = R_{ji} g^{1n[m_j/m_i]} = R_{ji}[m_j/m_i]^p \quad \text{(A2)}$$

where $p = \ln[g]$. This is the exponential law as expressed by Russell et al. (1978).

We note that Eqn. 4 is similar in appearance to the so-called 'generalized power law' derived by Maréchal et al. (1999). However the presence of the integral mass factor in the exponent in Eqn. 4 provides a more straightforward way to derive the exponential law.